JOURNAL OF SOLID STATE CHEMISTRY **121,** 251–261 (1996)
ARTICLE NO. 0036

Study of the Formation of $Bi_2Te_4O_{11}$

Zs. Szaller

Research Laboratory for Crystal Physics, Hungarian Academy of Sciences, 1502 Budapest,Pf.132, Hungary

L. Pöppl

Institute of Inorganic and Analytical Chemistry of L.Eötvös University, 1518 Budapest,112 Pf.32, Hungary

Gy. Lovas and I. Dódony

Mineralogical Department of L.Eötvös University 1088 Budapest, Múzeum krt. 4/a, Hungary

Received March 6, 1995; in revised form June 27, 1995; accepted July 7, 1995

The solid state reaction in a 1 : 4 mole ratio mixture of Bi_2O_3 and TeO_2 and the polymorphic phase transition of $Bi_2Te_4O_{11}$ have been investigated using differential scanning calorimetry (DSC), electron microprobe, X-ray powder diffraction (XPD), and selected area electron diffraction (SAED) analysis in the 25–730°C temperature range. Upon heating first a $8Bi_2Te_4O_{11} + 23TeO_2$ eutectic is formed, which melts at 598.9°C. In this melt the excess of Bi_2O_3 reacts further and the $Bi_2O_3 + 4TeO_2 = Bi_2Te_4O_{11}$ reaction takes place. The cubic modification is formed by fast crystallization of the $Bi_2Te_4O_{11}$ melt. The structure of the cubic $Bi_2Te_4O_{11}$ can be characterized by the lattice constant of $a = 5.6397(5)$ Å and space group $Fm3m$. The main product of a slow cooling is the same cubic polymorph although a subordinate formation of the monoclinic phase is also observed. The β-$Bi_2Te_4O_{11}$ cubic phase undergoes a monotropic transformation into the α-$Bi_2Te_4O_{11}$ monoclinic modification at temperatures higher than 400°C. The cubic → monoclinic transition is the result of an ordering in one set of {111} planes and the orthogonality of the cubic phase in the [110] projection changes to monoclinic symmetry. The melting enthalpies of the cubic β-phase and the monoclinic α-phase are 35.9 ± 3.3 J/g and 84.3 ± 4.3 J/g respectively.

INTRODUCTION

Bismuth-oxide-based compounds have a number of important applications such as in high-T_c superconductors (1), oxygen ion conductors (2, 3), and nonlinear optical materials (4). Among the nonlinear optical materials there are sillenites related to γ-Bi_2O_3, such as bismuth germanate, and its silicate and titanate counterparts, and δ-Bi_2O_3-type compounds such as bismuth tellurites ($Bi_2Te_4O_{11}$ and Bi_2TeO_5). The latter are also known as photorefractive (5–10) and acousto-optical materials (11) and might also have applications as oxygen ion conductors. For single-crystal growth of bismuth tellurites it is important to know the details of the solid state reaction between Bi_2O_3 and TeO_2. There are some contradictions in the published phase diagrams of this reaction (12, 13). In spite of the fact that bismuth tellurites can easily be oxidized in air there are still some open questions concerning the oxidation process (12–14). Bismuth tellurium oxide compounds have anion-deficient fluorite structures. It is not yet clear whether complete oxidation leading to the filling of all vacant oxygen sites is possible.

The chemical reaction between Bi_2O_3 and TeO_2 can be described by the following equation:

$$(1 - x)/2Bi_2O_3 + xTeO_2 = Bi_{1-x}Te_xO_{(3+x)}/2.$$

$Bi_2Te_4O_{11}$ ($x = 0.667$) is the first compound formed in the solid state reaction of Bi_2O_3 and TeO_2. The structure of $Bi_2Te_4O_{11}$ was first studied by Frit *et al.* (17) and the complete structure analysis was carried out by Rossel *et al.* (18). These authors described only the monoclinic α-modification. Demina *et al.* (15) reported on X-ray investigation of bismuth tellurites but they did not find polymorphic modifications either. The existence of a cubic β-polymorph of $Bi_2Te_4O_{11}$ above 609°C was first reported by Astaf'ev *et al.* (16), but no structural details of this phase were given. In the present paper the synthesis and properties of $Bi_2Te_4O_{11}$, in particular for the almost unknown β-modification, are discussed in detail.

EXPERIMENTAL

Starting materials were Bi_2O_3 (Johnson Matthey Grade 1) and TeO_2 prepared from tellurium metal (99.999%) by oxidation with HNO_3 (Carlo Erba for analysis). After a short anneal in air at 450°C the oxides were

0022-4596/96 $18.00

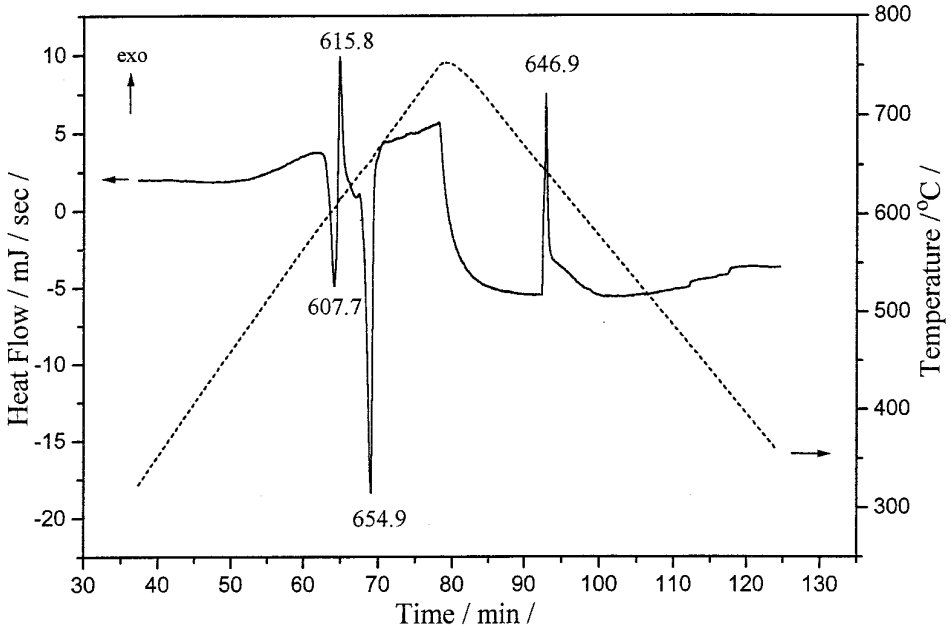

FIG. 1. DSC curve of a Bi_2O_3 + $4TeO_2$ mixture.

ground and sieved. The fraction with a grain size smaller than 63 μm was used for the synthesis and for the DSC measurements.

For X-ray powder diffraction (XPD) and selected area electron diffraction (SAED) analysis three samples of $Bi_2Te_4O_{11}$ were prepared (Samples A, B, and C). Sample A was made of a Bi_2O_3 + $4TeO_2$ mixture. The mixture was put into a platinum crucible, heated in a furnace up to 720°C under argon atmosphere, and kept 2 hr at this temperature with subsequent cooling to room temperature at 10°C/min. Sample B was prepared under the same conditions except for a different cooling rate (0.5°C/min). Sam-

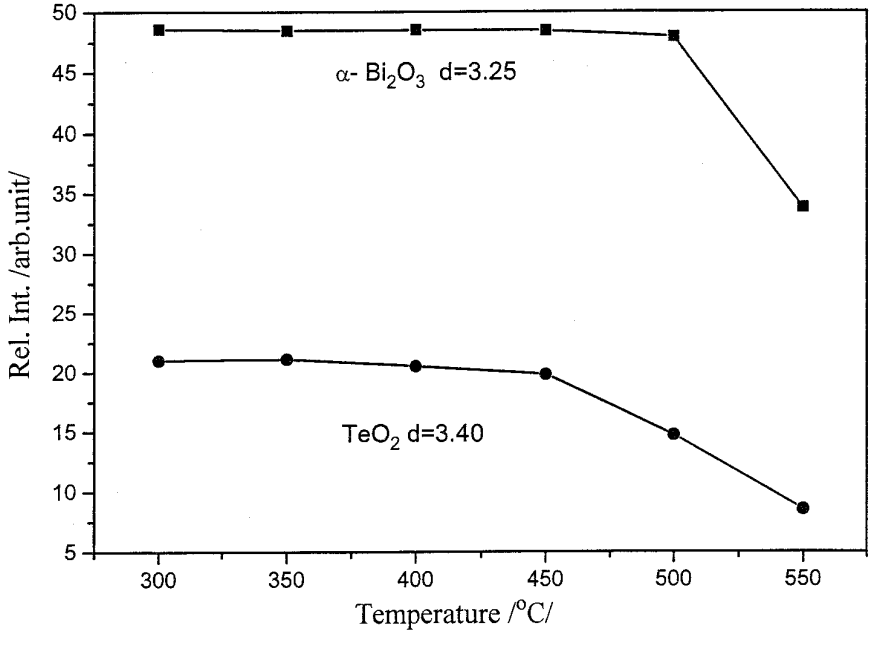

FIG. 2. Intensities of *d*-lines of oxides heated to different temperatures.

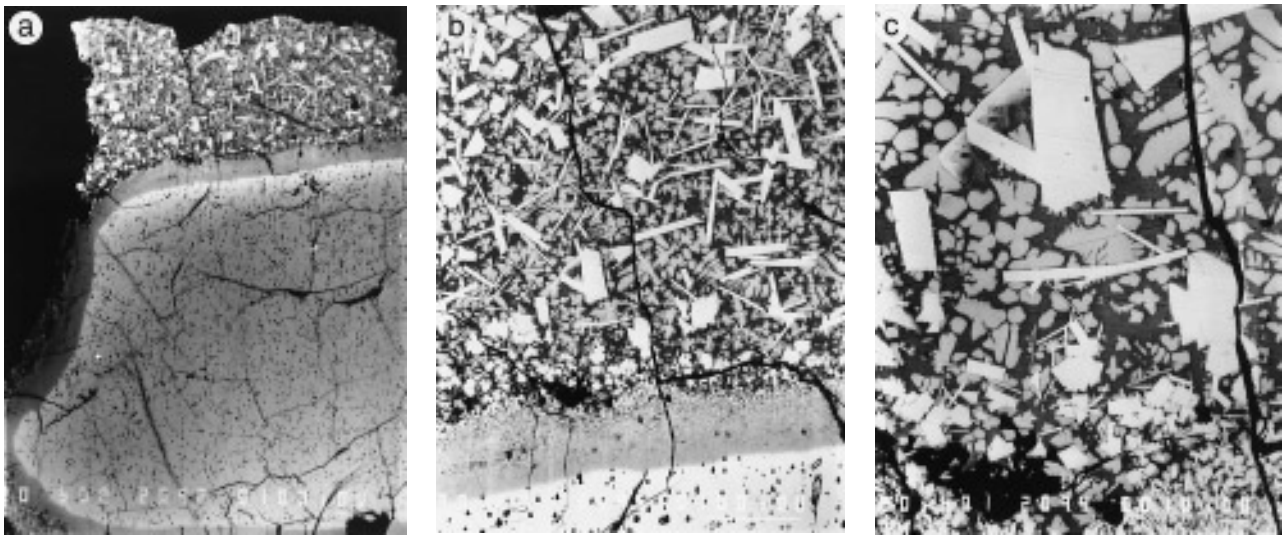

FIG. 3. Back-scattered electron pictures of the cross section of a pellet heated at 650°C for 60 min. (a) Unreacted Bi_2O_3 (bottom of the picture), solidified melting phase (top of the picture), and the microcrystalline $Bi_2Te_4O_{11}$ between them. Scale, 100 μm. (b) Magnified details of solidified melting phase. White prismatic and needle-like crystals have $Bi_2Te_2O_7$ composition, the gray dendrite-like crystals have $Bi_2Te_4O_{11}$ composition. Scale, 100 μm. (c) Magnified details of (b). Scale 10 μm.

ple C was prepared like Sample A but in a second heating cycle it was annealed at 500°C.

For electron microprobe analysis a pellet was prepared from Bi_2O_3 powder and annealed at 800°C in air. The pellet was polished, pressed with polished TeO_2 single crystal, and annealed for 1 hr at 650°C with subsequent quenching in argon atmosphere. This sample was broken into two pieces. The broken area was polished. The cross section was analyzed with a Jeol Microprobe 733 instrument using an accelerating voltage of 20 kV and a beam current of 20 mA. Bi_2O_3 and TeO_2 were used as standards and ZAF correction was applied.

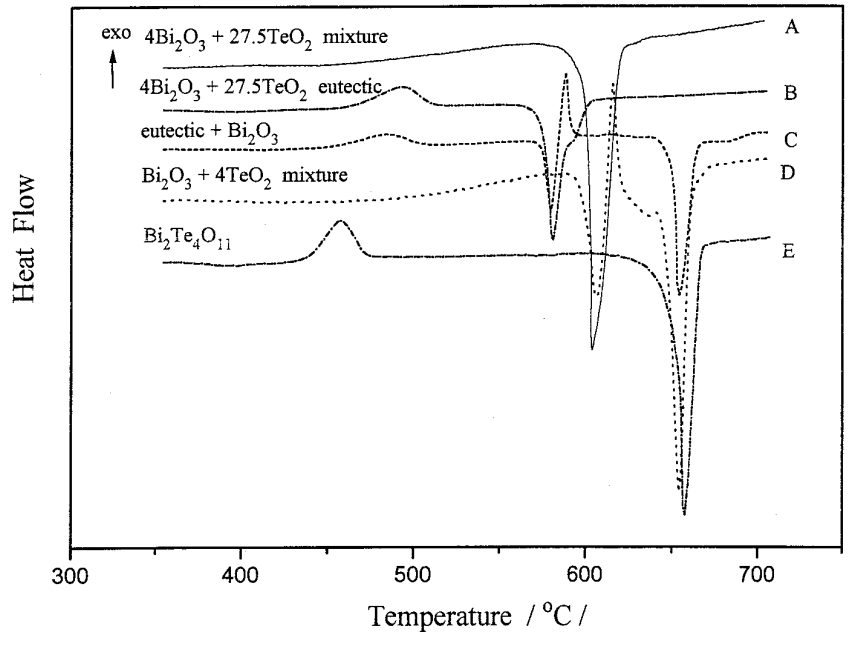

FIG. 4. DSC curves of different samples demonstrating the formation of $Bi_2Te_4O_{11}$.

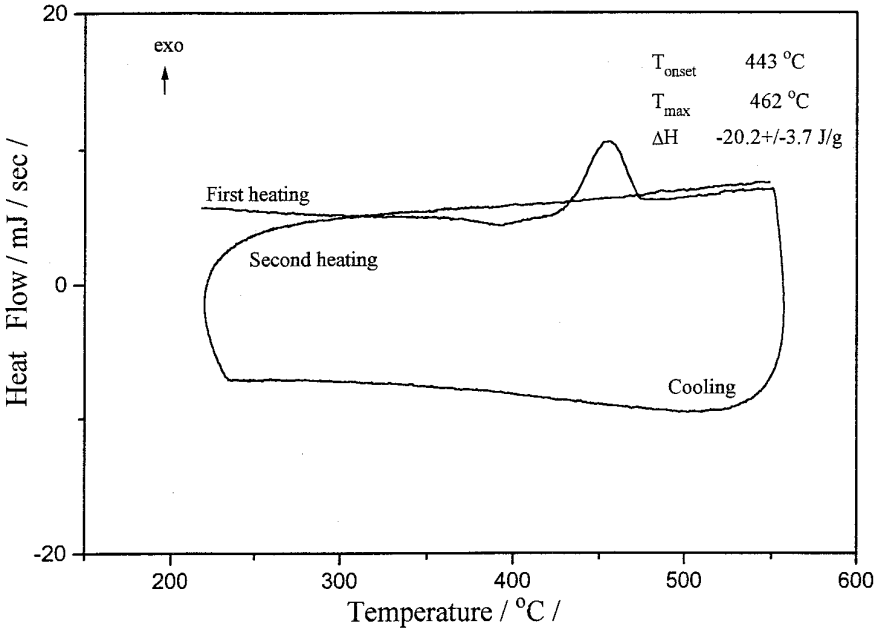

FIG. 5. DSC curve of the phase transition of cubic $Bi_2Te_4O_{11}$ modification showing the irreversibility of the monotropic transformation.

The DSC measurements were carried out by a PL Thermal Sciences 1500 Differential Scanning Calorimeter (DSC) in flowing argon atmosphere (10 ml/min), using 10°C/min heating and cooling rates. In the course of the determination of the melting enthalpy and melting point of α-$Bi_2Te_4O_{11}$, the heating was performed at a rate of 1°C/min in flowing argon atmosphere. For the temperature and the enthalpy calibration of the instrument, ICTA standards were used. All enthalpy results shown are the mean of from three to five runs and errors are calculated from range estimates of the results.

X-ray powder diffraction experiments were carried out

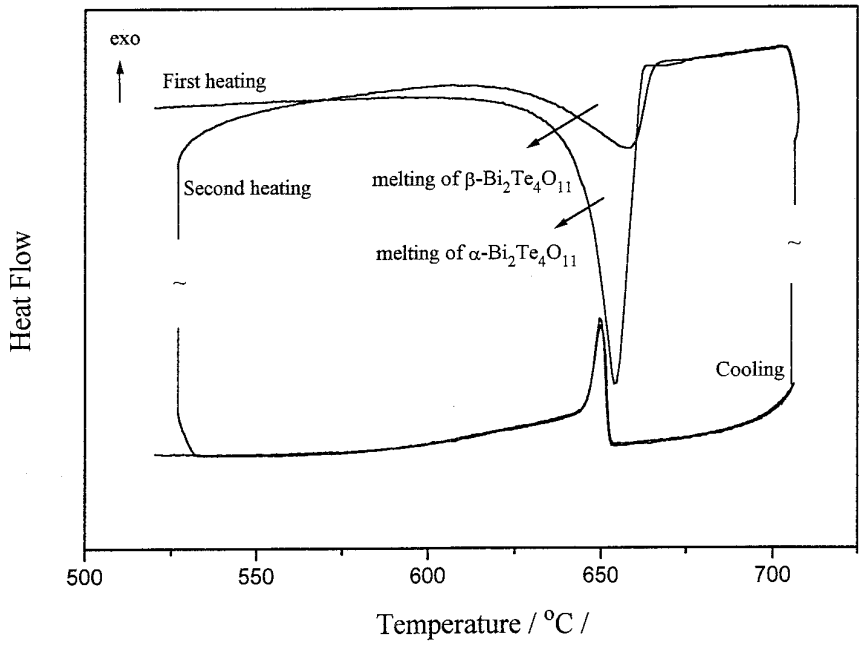

FIG. 6. DSC curve of the melting characteristics of α- and β-$Bi_2Te_4O_{11}$.

TABLE 1
Thermoanalytical Results of DSC Measurements

	Endothermic			Exothermic			Endothermic		
	T_{onset} (°C)	T_{max} (°C)	ΔH (J/g)	T_{onset} (°C)	T_{max} (°C)	ΔH (J/g)	T_{onset} (°C)	T_{max} (°C)	ΔH (J/g)
4:27.5 mixture	601.5	604.0	90.5 ± 2.1						
4:27.5 eutectic	575.3	580.5	89.9 ± 2.2						
Eutectic + Bi_2O_3	574.1	579.6	10.6 ± 1.1	584.4	588.8	−6.4 ± 1.2	650.9	653.7	37.8 ± 1.7
1:4 mixture	598.9	607.7	8.9 ± 1.1	612.5	615.8	−4.2 ± 1.1	646.7	654.9	44.0 ± 2.1
α-$Bi_2Te_4O_{11}$							650.8	655.3	84.3 ± 4.3
β-$Bi_2Te_4O_{11}$							626.7	658.7	35.9 ± 3.3
Solidification of β-$Bi_2Te_4O_{11}$				655.2	651.6	−32.5 ± 1.1			

from these samples using Cu-radiation ($\lambda_{CuK\alpha}$ = 0.154178 nm) on a Siemens D5000 powder diffractometer system using theta–theta geometry. The system was equipped with a pyrolytic graphite curved crystal secondary monochromator. Data collection and all subsequent calculations were performed on the integrated computing facilities of the D5000 system. The intensity data were collected with the step-scan technique in the 5–65° and 22–110° 2Θ ranges, using 0.02° 2Θ stepwidth.

SAED measurements of the above-mentioned samples were performed on a JEOL JEM 100CX transmission electron microscope applying a 100 kV accelerating voltage. Selected grains were oriented with their main crystallographic axis parallel to the beam using a side-entry tilt (±60°)-rotating (±360°) goniometer stage.

The chemical composition of $Bi_2Te_4O_{11}$ was determined by dissolution in HCl and bismuth and tellurium contents were measured by Zeiss AAS3 Atomic Absorp-

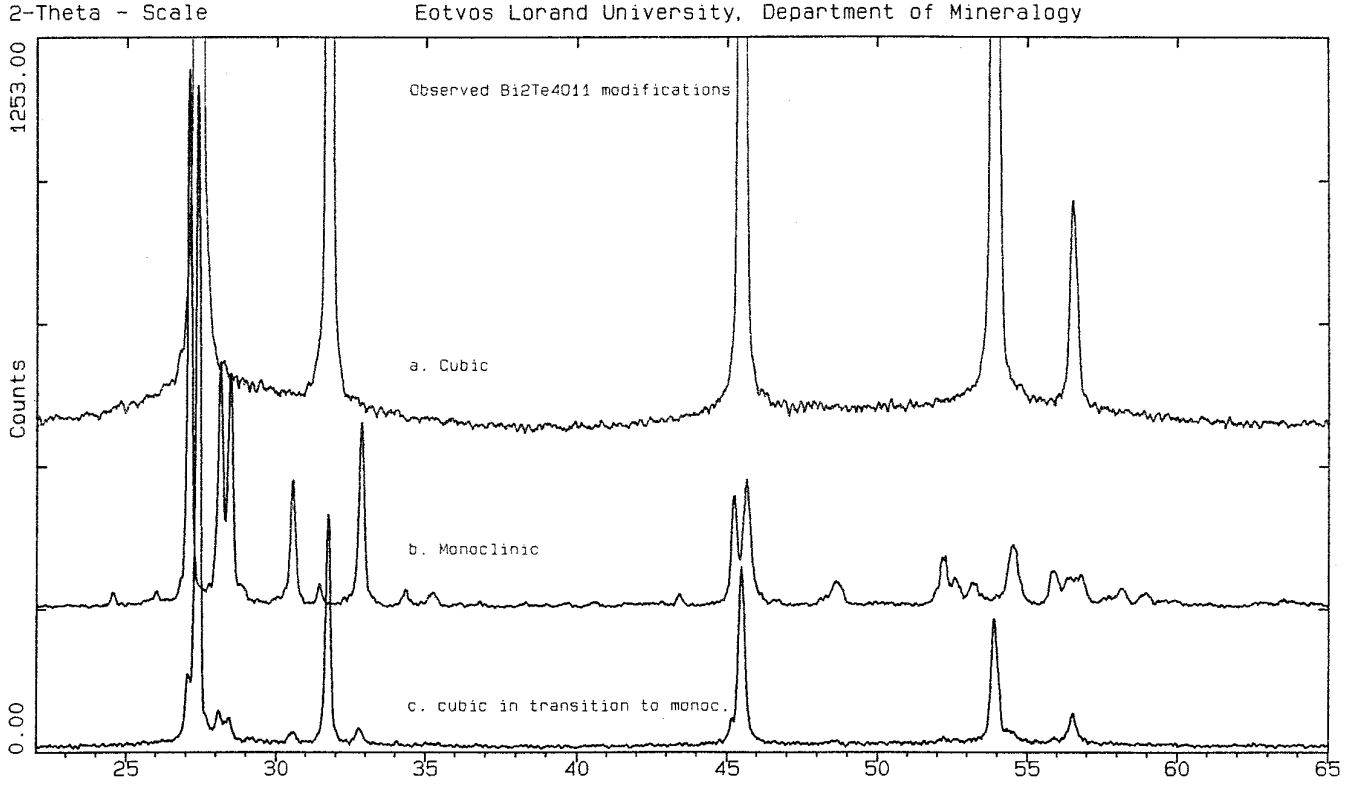

FIG. 7. X-ray powder pattern of different modifications of $Bi_2Te_4O_{11}$. (a) X-ray powder pattern of cubic $Bi_2Te_4O_{11}$. (b) X-ray powder pattern of monoclinic $Bi_2Te_4O_{11}$. (c) X-ray powder pattern of the coexistence of both modifications.

tion and PSX 75 Sequential ICP AES spectrometers, respectively.

The density measurement was carried out in a picnometer with carbon tetrachloride at 21°C.

RESULTS

Preliminary Examinations and Observations

The most characteristic features of the solid state reaction of the Bi_2O_3 + $4TeO_2$ mixture investigated by DSC can be seen in Fig. 1. Heating up the sample the base line remains stable up to 450°C, but above this temperature an exothermic shift can be observed. Then an endothermic process takes place at 607.7°C peak maximum, upon which an exothermic one at 615.8°C is superimposed. A second endothermic process can be seen at 654.9°C peak maximum. Only one sharp exothermic peak with a long tail on the lower temperature side can be observed during cooling of the sample.

To elucidate the origin of these DSC traces further experiments were carried out. From the exothermic baseline shift it could be expected that the reaction commences below 600°C. In order to prove this the Bi_2O_3 + $4TeO_2$ mixtures were heated to 300, 350, 400, 450, 500, and 550°C, respectively, in a Mettler TA-1 thermobalance under argon atmosphere, and kept for 30 min at these temperatures. After preparation the samples were examined by X-ray powder diffractometry supposing that the onset temperature of the reaction can be estimated from the decreasing *d*-line intensities (d = 3.25 Å for α-Bi_2O_3 and d = 3.40 Å for TeO_2) of the oxides. The results can be seen in Fig. 2. The amount of Bi_2O_3 decreases significantly above 500°C, while the diffraction line intensity of TeO_2 starts to decrease from 450°C and less than 50% of the oxide is present at 550°C. Our measurements confirm that the reaction among the two oxides starts near 450°C and the product should be a TeO_2-rich compound. The thermal motion of the atoms is considered as constant in this temperature range. The first endothermic peak on the DSC curve can be considered as a melting process. This was confirmed by optical microscope using a heated sample holder. Localized melting was observed at 600°C, then the sample solidified and melted again. The substance was a metallic gray color when cooled to room temperature.

Phase Identification by Electron Microprobe Analyses

Electron microprobe analyses were performed to identify the different phases existing in the course of Bi_2O_3 + $4TeO_2$ reaction. Results of these measurements cannot be strictly correlated with $Bi_2Te_4O_{11}$ formation, because the reaction could only take place within the contact surface layer and the mole ratio varies locally.

The back-scattered electron pictures in Figs. 3a–3c were taken from the cross section of the sample. Surprisingly, unreacted TeO_2 could not be identified, it was fully consumed. The analysis confirmed that the composition of the homogeneous phase with light color at the bottom of Fig. 3a is unmodified Bi_2O_3 reactant. At the top of the picture

TABLE 2
Powder Data and Unit Cell Refinement Results for β-$Bi_2Te_4O_{11}$ (Cubic)

	Unit cell dimensions	
	a	Volume
Reciprocal cell	0.177314D + 00	0.557488D − 02
Direct cell	0.563978D + 01	0.179375D + 03
	a	Volume
Reciprocal cell standard errors	0.177063D − 04	
Direct cell standard errors	0.563165D − 03	0.537352D − 01

n	*h*	*k*	*l*	d_{obs}	I/I_o	2Th(calc)	2Th(obs)	2Th(diff)	Figure of merit
1	1	1	1	3.260	100	27.390	27.354	0.0361	F 1 = 28(0.036, 1)
2	2	0	0	2.823	37	31.731	31.689	0.0421	F 2 = 26(0.039, 2)
3	2	2	0	1.997	28	45.488	45.446	0.0425	F 3 = 25(0.040, 3)
4	3	1	1	1.702	22	53.917	53.871	0.0467	F 4 = 24(0.042, 4)
5	2	2	2	1.6293	6	56.524	56.475	0.0496	F 5 = 23(0.043, 5)
6	4	0	0	1.4098	2	66.231	66.235	−0.0040	F 6 = 27(0.037, 6)
7	3	3	1	1.2937	4	73.074	73.077	−0.0021	F 7 = 31(0.032, 7)
8	4	2	0	1.2607	4	75.296	75.319	−0.0222	F 8 = 33(0.031, 8)
9	4	2	2	1.1510	2	83.997	84.010	−0.0127	F 9 = 35(0.029, 9)
10	5	1	1	1.0852	2	90.421	90.437	−0.0157	F10 = 37(0.027, 10)
11	4	4	0	0.9968	1	101.180	101.191	−0.0105	F11 = 39(0.026, 11)
12	5	3	1	0.9531	1	107.807	107.828	−0.0200	F12 = 39(0.025, 12)

TABLE 3
Powder Data and Unit Cell Refinement Results for α-$Bi_2Te_4O_{11}$ (Monoclinic)[a]

	Unit cell dimensions						
	a	*b*	*c*	Alpha	Beta	Gamma	Volume
Reciprocal cell	0.53117D − 01	0.12549D + 00	0.14371D + 00	90.0	8458.5	90.000	0.954357D − 03
Direct cell	0.18898D + 02	0.79683D + 01	0.69848D + 01	90.0	951.5	90.000	0.104782D + 04
	a	*b*	*c*	Alpha	Beta	Gamma	Volume
Reciprocal cell standard errors	0.756065D − 05	0.29160D − 04	0.25985D − 04	0.0	0.9	0.0	
Direct cell standard errors	0.279406D − 02	0.18515D − 02	0.12223D − 02	0.0	0.9	0.0	0.242303D + 00

n	*h*	*k*	*l*	d_{obs}	2Th(calc)	2Th(obs)	2Th(diff)	Figure of merit
2	2	0	0	9.434	9.395	9.374	0.021	F 1 = 24(0.021, 2)
8	−2	1	0	6.086	14.564	14.555	0.009	F 2 = 17(0.015, 8)
11	0	1	1	5.247	16.916	16.896	0.020	F 3 = 16(0.017, 11)
13	1	1	1	4.950	17.864	17.919	−0.055	F 4 = 12(0.026, 13)
16	−2	1	1	4.718	18.827	18.809	0.018	F 5 = 13(0.025, 16)
19	2	1	1	4.460	19.925	19.906	0.019	F 6 = 13(0.024, 19)
20	−3	1	1	4.155	21.358	21.386	−0.027	F 7 = 14(0.024, 20)
29	−4	1	1	3.626	24.573	24.550	0.023	F 8 = 11(0.024, 29)
31	−1	0	2	3.474	25.627	25.640	−0.013	F 9 = 13(0.023, 31)
32	0	2	1	3.466	25.766	25.700	0.066	F10 = 12(0.027, 32)
34	−1	2	1	3.426	25.998	26.005	−0.007	F11 = 13(0.025, 34)
41	−2	2	1	3.292	27.084	27.085	−0.001	F12 = 13(0.023, 41)
46	2	0	2	3.173	28.112	28.123	−0.011	F13 = 13(0.022, 46)
49	6	0	0	3.138	28.445	28.443	0.002	F14 = 14(0.021, 49)
54	3	2	1	2.971	30.046	30.080	−0.034	F15 = 13(0.022, 54)
60	−4	0	2	2.927	30.586	30.536	0.050	F16 = 11(0.024, 60)
62	−4	2	1	2.846	31.430	31.428	0.002	F17 = 12(0.022, 62)
68	4	2	1	2.727	32.800	32.836	−0.035	F18 = 11(0.023, 68)
75	6	1	1	2.613	34.262	34.319	−0.057	F19 = 10(0.025, 75)
82	4	1	2	2.545	35.243	35.261	−0.018	F20 = 10(0.024, 82), M20 = 6
84	5	2	1	2.488	36.022	36.096	−0.074	F21 = 9(0.027, 84)
93	−3	3	0	2.442	36.741	36.797	−0.056	F22 = 8(0.028, 93)
101	8	0	0	2.352	38.244	38.258	−0.014	F23 = 8(0.028, 101)
108	−4	3	0	2.314	38.933	38.920	0.013	F24 = 8(0.027, 108)
113	6	2	1	2.275	39.618	39.607	0.011	F25 = 8(0.026, 113)
121	−7	0	2	2.223	40.559	40.576	−0.017	F26 = 8(0.026, 122)
136	2	1	3	2.127	42.491	42.502	−0.011	F27 = 8(0.025, 136)
145	−2	3	2	2.084	43.425	43.412	0.013	F28 = 8(0.025, 145)
162	0	2	3	2.004	45.237	45.233	0.004	F29 = 7(0.024, 162)
166	−9	1	1	1.987	45.620	45.647	−0.027	F30 = 7(0.024, 166)
180	−6	0	3	1.948	46.611	46.625	−0.013	F31 = 7(0.024, 180)
199	3	2	3	1.871	48.724	48.664	0.060	F32 = 6(0.025, 199)
221	4	2	3	1.794	50.800	50.845	−0.045	F33 = 6(0.026, 221)
230	−6	2	3	1.751	52.216	52.209	0.007	F34 = 6(0.025, 230)
236	−2	0	4	1.739	52.618	52.597	0.021	F35 = 6(0.025, 236)
246	−10	0	2	1.720	53.210	53.207	0.003	F36 = 6(0.024, 246)
272	−6	4	0	1.682	54.518	54.524	−0.006	F37 = 6(0.024, 273)
288	−9	3	0	1.644	55.903	55.875	0.028	F38 = 5(0.024, 288)
293	11	0	1	1.630	56.433	56.406	0.027	F39 = 6(0.024, 293)
298	7	3	2	1.621	56.806	56.736	0.070	F40 = 5(0.025, 298)
309	11	1	1	1.596	57.709	57.711	−0.002	F41 = 5(0.025, 309)
317	9	2	2	1.585	58.168	58.150	0.018	F42 = 5(0.025, 317)
329	10	1	2	1.566	58.888	58.907	−0.019	F43 = 5(0.025, 329)
340	−4	2	4	1.548	59.676	59.661	0.015	F44 = 5(0.024, 340)
397	−4	4	3	1.463	63.522	63.540	−0.018	F45 = 5(0.024, 397)

[a] Space group $P2_1$ after E. Spiridonov *et al, Moscow Univ. Geology Bull.* **42**(6), 71 (1987).

there is a heterogeneous phase which shows a very complex morphological structure. Between these regions a light-gray layer can be observed. Investigating the heterogeneous phase with higher magnifications (Figs. 3b and 3c) it is revealed to consist of three well-distinguishable compounds. The dark background is a solidified melt phase consisting of $4Bi_2O_3 + 29TeO_2$. The gray dendrite-like crystals with rounded outline boundary have a composition of $Bi_2O_3 + 4TeO_2$ ($Bi_2Te_4O_{11}$). The white prismatic and needle-like crystals are identified as $Bi_2O_3 + 2TeO_2$ ($Bi_2Te_2O_7$). The light-gray layer consists of microcrystalline $Bi_2Te_2O_7$.

Study of $Bi_2Te_4O_{11}$ Formation by DSC

According to the phase diagram of the $Bi_2O_3 - TeO_2$ system (12) the $4Bi_2O_3 + 27.6TeO_2$ eutectic has the lowest melting point. This eutectic is a mixture of $Bi_2Te_4O_{11}$ and TeO_2 as confirmed by X-ray diffraction analysis. The accurate value of the eutectic composition was determined by DSC and it was found to be $8Bi_2Te_4O_{11} + 23TeO_2$ or $4Bi_2O_3 + 27.5TeO_2$. To prove that the first endothermic peak at 607.7°C peak maximum in Fig. 1 arises from the melting of eutectic, an analysis of the $4Bi_2O_3 + 27.5TeO_2$ mixture was carried out. In the course of heating the eutectic was formed and melted at 601.5°C (Fig. 4, Curve A). If already present the melting point of the eutectic is 575.3°C (Curve B). It was consistent during the experimental work that the melting temperature of the eutectic depends strongly on the nature of the reactants. If the starting materials were pure oxides the melting temperature of the eutectic was always higher (Curves A and D in Fig. 4.). The explanation is that the chemical (i.e., oxide) composition of the eutectic is $4Bi_2O_3 + 27.5TeO_2$, but $Bi_2Te_4O_{11}$ and TeO_2 are the compounds which form the eutectic. Namely if $Bi_2Te_4O_{11}$ is not present as reactant it has to be formed and the melting temperature will be higher. But if $Bi_2Te_4O_{11}$ is already present the real melting temperature of the eutectic can be measured (curve B and C in Fig. 4.).

To show that the origin of the exothermic peak in Fig. 1 is due to the reaction of unreacted Bi_2O_3 with the TeO_2 content of the eutectic we added the stoichiometric quantity of Bi_2O_3 needed for the formation of $Bi_2Te_4O_{11}$ to the eutectic. The obtained DSC curve (Curve C) is similar to that of the $Bi_2O_3 + 4TeO_2$ mixture (Curve D), but the endothermic and exothermic peaks are obtained at lower temperatures.

In both cases the chemical reaction proceeds faster in the molten phase so the formation of $Bi_2Te_4O_{11}$ is completed with accompanying heat release. The crystalline $Bi_2Te_4O_{11}$ melts at 650.8°C. We summarize the thermoanalytical results in Table 1.

The chemical sequence of $Bi_2Te_4O_{11}$ formation as deduced from the results given above:

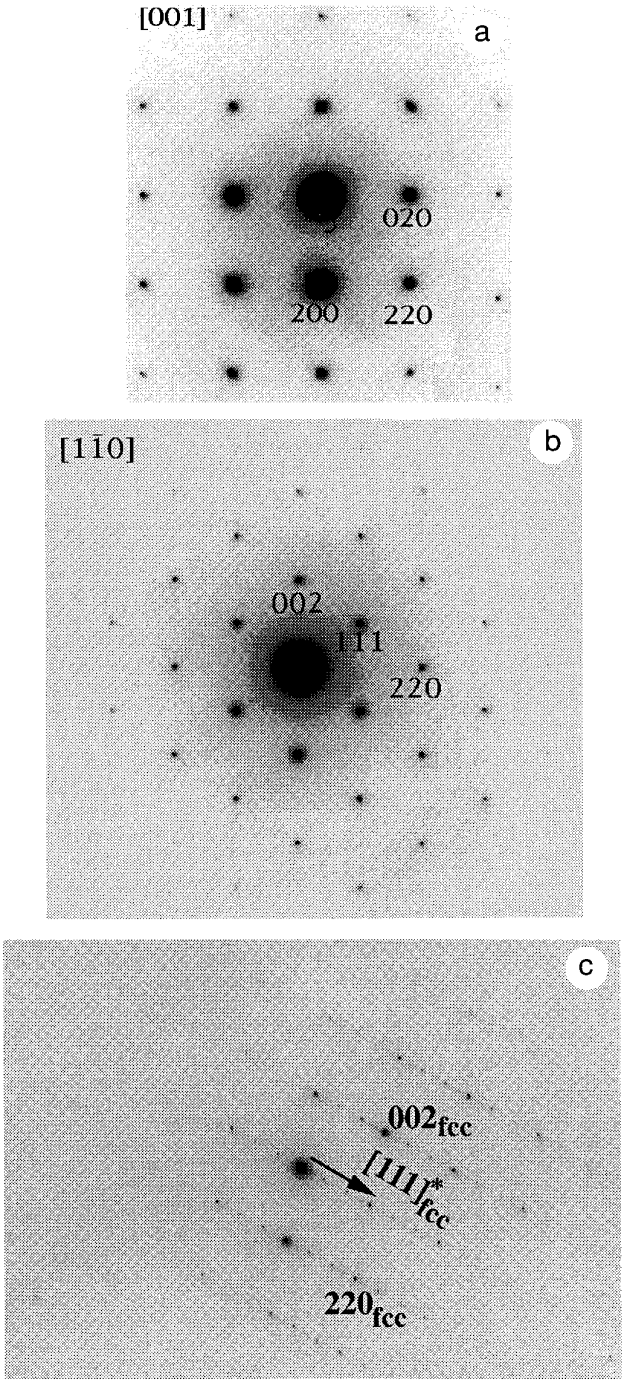

FIG. 8. SAED patterns of $Bi_2Te_4O_{11}$ modifications. (a) [001] projected SAED patterns of the cubic $Bi_2Te_4O_{11}$ modification. (b) [1 $\bar{1}$ 0] projected SAED patterns of the cubic $Bi_2Te_4O_{11}$ modification. (c) Superstructure of fcc sublattice.

Step 1. $Bi_2Te_4O_{11}$ forms above 450°C, which is probably a diffusion-controlled reaction.

Step 2. When the amount of $Bi_2Te_4O_{11}$ is sufficient the ($8Bi_2Te_4O_{11} + 23TeO_2$) eutectic is formed.

Step 3. Melting of the eutectic.

TABLE 4
Unit Cell Parameters of α-$Bi_2Te_eO_{11}$ (Monoclinic)

Reference	a [Å]	b [Å]	c [Å]	β	Density (calc.) (g/cm^3)
Frit (17)	19.107(5)	7.971(5)	6.904(5)	95.74(5)	7.01
Demina (15)	19.11(1)	7.995(6)	6.910(6)	95.78(5)	7.01
Chekhovichite natural	19.00	7.982	6.938	95.67	6.88
mineral, Spiridonov (23)	18.89	7.968	9.919	95.89	
Astaf'ev (16)	18.894	7.960	6.974	95.30	7.04
Rossel (18)	18.8963(8)	7.9593(3)	6.9909(3)	95.176(3)	7.00
Present work	18.898(3)	7.968(2)	6.985(1)	95.025(15)	7.00

Step 4. The formation of $Bi_2Te_4O_{11}$ is completed in the molten phase.

Step 5. Melting of $Bi_2Te_4O_{11}$.

Study of the Polymorphic Transition of $Bi_2Te_4O_{11}$ by DSC

In our preparation process when the sample was cooled down from the melt by 10°C/min (Sample A) only cubic modification could be obtained. The detailed X-ray diffraction analysis is described in the next section. The most obvious feature identified for the cubic phase was the exothermic peak on the heating curve at about 450°C (Fig. 4, Curve E). Figure 5 shows the results of a heating–cooling–heating cycle below the melting point. There is no DSC peak for the second heating. We checked the structure of the sample after the DSC measurement by X-ray diffraction and the monoclinic form was identified. Once the monoclinic modification is formed it cannot be transformed to cubic phase below the melting point in either the heating or the cooling process. Thus it is obvious that this exothermic process is an irreversible monotropic transformation from cubic to monoclinic phase. Accordingly the monoclinic modification is the stable form of $Bi_2Te_4O_{11}$ and the cubic is the metastable one. In accordance with Oswald's rule, the least stable modification often forms from the melts of polymorphic substances on cooling.

The melting point and the melting enthalpy normally measured belongs to the monoclinic phase. However, cooling the melt to just below the solidification temperature (~500–530°C) and heating it again, the second melting process is due to the cubic phase. Figure 6 shows the results. It can be established that the measured heat of crystallization is equal to the heat of fusion for the cubic form and the solidification temperature and enthalpy of the monoclinic form could not be detected. It also explains the formation of cubic modification in every cooling process. The accurate value of the melting point and the melting enthalpy of the β-$Bi_2Te_4O_{11}$ modifications could not be determined because the cubic phase transformed into monoclinic phase when the heating rate was lower than 10°C/min. The determined melting point and melting enthalpy of α- and β-$Bi_2Te_4O_{11}$ using 1°C/min and 10°C/min heating rates are summarized in Table 1.

Results of the Chemical Analysis and Density Measurement

The results of the chemical analysis of $Bi_2Te_4O_{11}$ are the following: bismuth content is 11.66 ± 0.12 mole% (theoretical concentration 11.765 mole%), tellurium content is 22.7 ± 0.7 mole% (theoretical concentration 23.530 mole%).

The density of β-$Bi_2Te_4O_{11}$ was found to be 6.81 ± 0.02 g/cm^3.

Study of the Polymorphic Modifications using XPD and SAED Analysis

The crystallographic study of the $Bi_2Te_4O_{11}$ (Sample A) was carried out by X-ray diffraction. The powder pattern of this material is shown in Fig. 7a. An attempt of a phase analysis using the current ICDD-JCPDS database (19, 20) failed, indicating that there is not powder data for this phase. Following a data reduction (smoothing, background treatment, and peak search) performed by the integrated DIFFRAC-AT package of D5000, an indexing of the pattern was attempted using the ''Trial and Error'' technique as described by Werner (21). The solution with the highest consistency mark was a cubic unit cell with a dimension of 5.6 Å and volume of 179 Å^3. This unit cell was used in a subsequent cell refinement (22) and indexing using a locally modified version of the UNITCELL program of

TABLE 5
Unit Cell Parameters of β-$Bi_2Te_4O_{11}$ (Cubic)

Reference	a [Å]	Density (exp.) (g/cm^3)	Density (calc.) (g/cm^3)
Astaf'ev (16)	5.640	6.88 ± 0.05	6.82
Present work	5.6397(5)	6.81 ± 0.02	6.83

Appelman *et al.* (23). The final results of the refinement are given in Table 2. The results show that this material is a cubic modification of $Bi_2Te_4O_{11}$. The given unit cell suitably indexed all reflections and the indexing is consistent with the *Fm*3*m* space group. Calculations using the measured density, the formula confirmed by chemical analysis, and the unit cell volume showed that a fractional site occupancy can be expected in this structure. The powder pattern of Sample C can be seen in Fig. 7b. A phase analysis of this material using the ICDD-JCPDF database (19, 20) immediately led to the identification of the pure monoclinic modification of $Bi_2Te_4O_{11}$ described by Frit *et al.* (14). Subsequent to a data reduction, a unit cell refinement was launched using the $P2_1$ monoclinic structural model suggested by Spiridonov *et al.* (24). The final results shown in Table 3 indicated that this material—including the unit cell dimensions—is similar to the one described by Frit *et al.* (17), but shows differences from the data of Spiridonov *et al.* (24) as no traces of 100 reflection (18.9 Å) were found. Accordingly a more detailed structural investigation is indicated.

The powder pattern of Sample B is shown in Fig. 7c. The phase analysis of this sample showed that it was not a single-phase material but evidently a mixture of both modifications. The majority of the material consists of the cubic phase but distinct marks of the presence of the monoclinic structure can also be recognized. This kind of coexistence of both modifications indicates that even a fairly slow (0.5 C/min) cooling rate is insufficient to ensure a considerable transition from the cubic modification into the monoclinic one.

The SAED patterns proved the fcc symmetry of the $Bi_2Te_4O_{11}$ (Sample A). The [001] and [$1\,\bar{1}\,0$] projected SAED patterns of this phase are shown in Figs. 8a and 8b. The α-$Bi_2Te_4O_{11}$ crystals (Sample C) can be characterized by a superstructure of the fcc sublattice. The cubic → monoclinic transition is the result of an ordering in one set of {111} planes with periodicity of $3xd_{(111)fcc}$ (Fig. 8c). As a consequence of this ordering processes the orthogonality of the [110] projection vanishes and the structure changes to the monoclinic symmetry. The detailed crystallographic description of the phase transformation between the cubic and monoclinic phases is the aim of a subsequent paper.

CONCLUSION

By studying the solid state reaction under increasing temperature it can be established that Bi_2O_3 and TeO_2 react to a significant degree starting from 450°C. First $Bi_2Te_4O_{11}$ is formed. When the molar ratio of $Bi_2Te_4O_{11}$ and the unreacted TeO_2 reaches 8 : 23 ($4Bi_2O_3 : 27.5TeO_2$) it melts at 598.9°C. This composition is an eutectic and has the lowest melting point (575.3°C) in the bismuth oxide-tellur dioxide pseudo-binary system.

In the melt of the eutectic the reaction of still unreacted starting materials takes place ($Bi_2O_3 + 4TeO_2 = Bi_2Te_4O_{11}$). Increasing the temperature, $Bi_2Te_4O_{11}$ melts at 646.7°C. when the sample is cooled there is a tail exothermic peak on the DSC curve which shows a slow solidification process.

When the $Bi_2Te_4O_{11}$ melt is cooled, the cubic phase can form. Except for a partial conversion at an extremely slow (0.5°C/min) cooling rate this cubic phase cannot be transformed into a thermodynamically stable monoclinic modification because of kinetic hindrance. The cubic phase undergoes a monotropic transformation into the monoclinic above 400°C. This observation is in contrast with those of Astaf'ev *et al.* (16).

The two modifications have different melting points and melting enthalpies. The heat of fusion of the metastable cubic form is smaller than that of the stable monoclinic one and the melting point is also lower for the monoclinic form. The solidification temperature and enthalpy of the monoclinic form could not be detected.

The monoclinic $Bi_2Te_4O_{11}$ crystals are characterized by a superstructure of the fcc sublattice. The cubic monoclinic transition is the result of an ordering in one set of {111} planes with periodicity of $3xd_{(111)fcc}$. As a consequence of these ordering processes, the orthogonality of the [110] projection vanishes and the structure changes to monoclinic symmetry.

Finally, we summarize the unit cell parameters of both modifications published up to now (Tables 4 and 5).

ACKNOWLEDGMENTS

One of the authors (Zs. Szaller) was supported by a young scientist grant of the National Research Foundation for the (OTKA F-4357) and by a financial support of the Hungarian Science Foundation of the Hungarian Credit Bank. The analytical work of Dr. O. Szakacs is kindly acknowledged.

REFERENCES

1. R. J. Cava, in "Processing and Properties of High-T_c Superconductors" (Sungho Jin, Ed.), Vol. 1, p. 33. World Scientific, Singapore (1993).
2. E. C. Subbarao and H. S. Maiti, *Solid State Ionics* **11,** 317 (1984).
3. E. C. Subbarao and H. S. Maiti, in "Progress in Solid Electrolytes" (T. A. Wheat, A. Ahmad, and A. K. Kuriakose, Eds.). Canada Center for Mineral and Energy Technology, Ottawa (1983).
4. M. P. Petrov, S. I. Stepanov, and A. V. Khomenko, *in* "Photorefractive Crystals in Coherent Optical Systems" (T. Tamir, Ed.), Vol. 59, p. 233. Springer-Verlag, Berlin/Heidelberg (1991).
5. G. Mandula, L. Kovács, Á. Péter, and E. Hartman, *Opt. Mat.* **1,** 161 (1992).
6. G. Mandula, Á. Péter, and E. Hartman, *Pure Appl. Opt.* **3,** 839 (1994).
7. I. Földvári, Á. Péter, R. Voszka, and L. A. Kappers, *J. Cryst. Growth* **100,** 75 (1990).

8. S. A. Astaf'ev, A. A. Abdullaev, O. I. Vorob'eva, V. A. Dolgikh, A. Popovkin, I. M. Silvestrova, and E. M. Spiridonov, *Izv. Akad. SSSSR Neorg. Mater.* **27,** 60 (1991).
9. I. Földvári, M. P. Scripsick, L. E. Halliburton, and Á. Péter, *Phys. Lett. A.* **154,** 84 (1991).
10. I. Földvári, Á. Péter, L. A. Kappers, O. R. Gilliam, and R. Capelletti, *J. Mater. Sci.* **27,** 750 (1992).
11. V. A. Dolgikh and B. A. Popovkin, *Izv. Akad. Nauk. SSSR Neorg. Mater.* **4,** 748 (1978).
12. L. A. Demina, V. A. Dolgikh, B. A. Popovkin, and A. V. Novoselova, *Dokl. Akad. Nauk. SSSR Khim.* **1,** 94 (1979).
13. T. Kikuchi, Y. Kitami, M. Yokoyama, and H. Sakai, *J. Mater. Sci.* **24,** 4275 (1989).
14. B. Frit and M. Jaymes, *Bull. Soc. Chim. France* **3–4,** 402 (1974).
15. L. A. Demina and V. A. Dolgikh, *Zh. Neorg. Khim.* **4,** 949 (1984).
16. S. A. Astaf'ev, A. A. Abdullaev, V. A. Dolgikh, and B. A. Popovkin, *Izv. Akad. Nauk. SSSR Neorg. Mater.* **5,** 870 (1989).
17. B. Frit and M. Jaymes, *Rev. Chim. Miner.* **9,** 837–844 (1972).
18. H. J. Rossel, M. Leblanc, G. Férey, D. J. M. Bevan, D. J. Simpson, and M. R. Taylor, *Aust. J. Chem.* **45,** 1415 (1992).
19. "Powder Diffraction File PDF-1 ICDD-JCPDS 1601," Park Lane, Swarthmore, PA 19081 (1992).
20. "Powder Diffraction File PDF-2 ICDD-JCPDS 1601," Park Lane, Swarthmore, PA 19081 (1993).
21. P. W. Werner, *Z. Krist.* **120,** 375 (1964).
22. G. S. Smith and R. L. Snyder, *J. Appl. Crystallogr.* **12,** 60 (1979).
23. D. E. Appelman and H. T. Evans, Jr., "Job 9214: Indexing and Least-Squares Refinement of Powder Diffraction Data," Report PB2-16188, U.S. Dept. of Commerce, National Technical Information Service (1973).
24. E. M. Spiridonov, I. V. Petrova, L. A. Demina, V. I. Dolgikh, and G. M. Antonian, *Vestn. Mosk. Univ. Ser. 4. Geol.* **6,** 71 (1987).